

**MICROSTRUCTURE AND KINETIC GROWTH
OF ALUMINIDE COATING ON 304 STAINLESS
STEEL BY SLURRY ALUMINIZING**

TAN SIEW MIN

UNIVERSITI SAINS MALAYSIA

2022

**SCHOOL OF MATERIALS AND MINERAL RESOURCES ENGINEERING
UNIVERSITI SAINS MALAYSIA**

**MICROSTRUCTURE AND KINETIC GROWTH OF ALUMINIDE COATING
ON 304 STAINLESS STEEL BY SLURRY ALUMINIZING**

By

TAN SIEW MIN

Supervisor: Assoc. Prof. Ts. Ir. Dr. Anasyida bt. Abu Seman

Co-Superior: Dr. Tuti Katrina bt. Abdullah

Dissertation submitted in partial fulfillment of the requirements for the degree of

Bachelor of Engineering with Honours

(Materials Engineering)

Universiti Sains Malaysia

August 2022

DECLARATION

I hereby declare that I have conducted, completed the research work and written the dissertation entitled 'Microstructure and Kinetic Growth of Aluminide Coating on 304 Stainless Steel by Slurry Aluminizing'. I also declare that it has not been previously submitted for the award of any degree and diploma or other similar title of this for any other examining body or University.

Name of Student: Tan Siew Min

Signature:

Date: 12 August 2022

Witness by

Supervisor: Assoc. Prof. Ts. Ir. Dr. Anasyida

Signature:

bt. Abu Seman

Date: 12 August 2022

ACKNOWLEDGEMENT

First and foremost, I would like to express my deepest appreciation to Universiti Sains Malaysia for giving me an opportunity to complete my degree of Bachelor of Materials Engineering. Besides, I am highly indebted to School of Materials and Mineral Resources Engineering for providing the laboratory facilities and materials in order to conduct the experiment and obtain the necessary results for this project.

Moreover, I would like to express my sincere gratitude to my project supervisor, Assoc. Prof. Ts. Ir. Dr. Anasyida bt. Abu Seman, who always providing me valuable advice and guidance throughout this project. The goals of this project would not been achieved without her constant supervision, patience and support.

Furthermore, I would also like to thank Dr. Tuti Katrina bt. Abdullah and Mr. Muhammad Affifi bin Jamaluddin for willing to share their valuable time and knowledge throughout the entire period of this project.

Last but not least, I would like to express my gratitude towards my family members and friends for their kind encouragement and endless support which help me in the completion of this project.

TABLE OF CONTENTS

DECLARATION	ii
ACKNOWLEDGEMENT.....	iii
TABLE OF CONTENTS	iv
LIST OF TABLES	viii
LIST OF FIGURES	x
LIST OF SYMBOLS	xv
LIST OF ABBREVIATIONS	xvi
LIST OF APPENDICES	xvii
ABSTRAK	xviii
ABSTRACT.....	xix
CHAPTER 1 INTRODUCTION.....	1
1.1 Background	1
1.2 Problem Statement	2
1.3 Objective	4
1.4 Thesis Outline	4
CHAPTER 2 LITERATURE REVIEW	5
2.1 Introduction.....	5
2.2 Austenitic stainless steel	5
2.3 Aluminide coating.....	7
2.4 Aluminide coating technique - Slurry Aluminizing.....	8
2.5 General applications of aluminide coating.....	10
2.6 Slurry aluminizing process.....	12
2.7 Effect of temperature and time on aluminide coating.....	15
2.8 Growth kinetic of aluminide coating	20
2.9 Hardness.....	25

2.10	Corrosion behaviour of aluminide coating.....	27
CHAPTER 3 MATERIALS AND METHODOLOGY.....		32
3.1	Introduction.....	32
3.2	Raw Materials	32
3.2.1	Stainless steel 304	32
3.2.2	Aluminium powder (Al)	32
3.2.3	Alumina powder (Al ₂ O ₃)	33
3.2.4	Polyviynl alcohol (PVA).....	33
3.2.5	Distilled water (H ₂ O)	33
3.2.6	Ethanol (C ₂ H ₅ OH)	33
3.2.7	Polyviynl butyral (PVB)	33
3.2.8	Aluminium chloride (AlCl ₃)	34
3.2.9	Argon gas	34
3.3	Process flow	34
3.4	Methodology	36
3.4.1	Sample preparation	36
3.4.2	Selection of binder for slurry aluminide coating	37
3.4.3	Aluminide coating deposition	39
3.4.4	Heat treatment of aluminide slurry	40
3.4.5	Characterization	41
3.5	Raw material characterization.....	42
3.5.1	Particle size analyzer Malvern	42
3.6	Aluminide coating characterization	43
3.6.1	Sample preparation for aluminide coating characterization	43
3.6.2	Scanning Electron Microscope (SEM) tabletop.....	44
3.6.3	Field-Emission Scanning Electron Microscope-Energy Dispersive X-ray Spectroscopy (FESEM-EDX).....	45
3.6.4	X-ray diffraction (XRD)	45

3.6.5	Optical microscope	46
3.6.6	Nano hardness test	46
3.6.7	Potentiostat / Galvanostat	47
3.7	Growth kinetics of aluminide layer.....	47
CHAPTER 4 RESULTS AND DISCUSSION		48
4.1	Introduction.....	48
4.2	Raw material characterization.....	48
4.3	Selection of binder for slurry aluminide coating	50
4.3.1	SEM Tabletop Cross-Sectional Analysis.....	50
4.3.2	SEM-EDX Cross-Sectional Analysis	51
4.3.3	Phase identification of aluminide coating.....	53
4.3.4	Coating thickness of test sample.....	54
4.4	Aluminide coating.....	56
4.4.1	Surface image.....	56
4.4.2	SEM-EDX Cross-Sectional Analysis of Aluminide Coating	58
4.4.2(a)	Heat treatment at 600°C.....	58
4.4.2(b)	Heat treatment at 630°C	58
4.4.2(c)	Heat treatment at 650°C.....	62
4.4.2(d)	Heat treatment at 680°C.....	67
4.4.2(e)	Heat treatment at 700°C.....	71
4.4.3	Phase identification of aluminide coating.....	72
4.4.3(a)	Heat treatment at 600°C.....	72
4.4.3(b)	Heat treatment at 630°C.....	73
4.4.3(c)	Heat treatment at 650°C.....	74
4.4.3(d)	Heat treatment at 680°C.....	76
4.4.3(e)	Heat treatment at 700°C.....	77

4.4.4	Aluminide coating thickness.....	78
4.4.5	Growth kinetics of aluminide coating.....	81
4.4.6	Porosity measurement.....	84
4.4.7	Nano hardness test	85
4.4.8	Corrosion behaviour of aluminide coating.....	89
CHAPTER 5 CONCLUSIONS AND RECOMMENDATION.....		92
5.1	Conclusions.....	92
5.2	Recommendations.....	93
REFERENCES.....		94
APPENDICES		

LIST OF TABLES

	Page
Table 2.1: Different intermetallic compound and its Gibbs free energy (Dong <i>et al.</i> , 2019; Y. Yang <i>et al.</i> , 2018)	16
Table 2.2: Gibbs free energy for intermetallic compounds at temperature of 600°C, 630°C, 650°C, 680°C and 700°C.....	17
Table 2.3: Enthalpies of formation and activation energies for growth of various Fe-Al intermetallic phases (Dangi <i>et al.</i> , 2018)	22
Table 3.1: Mass and weight percentage for test sample PVA	38
Table 3.2: Mass and weight percentage for test sample PVB and PVB+2% AlCl ₃ ...	38
Table 3.3: Mass and weight percentage of slurry mixture for the project	39
Table 4.1: EDX chemical composition of the inner layer between the coating and substrate for test sample PVA, PVB and PVB+2% AlCl ₃	53
Table 4.2: The entire surface image of the aluminide coated sample.....	57
Table 4.3: EDX chemical composition of spectrum 1, 2, 3 and 4 for sample heat treated at 630°C for 10 hours	60
Table 4.4: EDX chemical composition of spectrum 1, 2, 3 and 4 for sample heat treated at 650°C for 10 hours	65
Table 4.5: EDX chemical composition of spectrum 1, 2, 3 and 4 for sample heat treated at 680°C for 10 hours	69
Table 4.6: Coating thickness and thickness of FeAl layer of sample with entirely Al and sample with 7Al : 3Al ₂ O ₃ slurry composition heat treated at 680 °C for 4 hours	79
Table 4.7: Maximum depth, hardness and reduced modulus of layer 1, 2, 3, 4 and 5 for sample after heat treatment at 700°C for 8 hours.....	88

Table 4.8: Corrosion potential, corrosion current and corrosion rate for sample heat treated at 650 °C , 680 °C and 700 °C for 8 hours and 10 hours respectively91

LIST OF FIGURES

	Page
Figure 2.1: Slurry aluminization steps by dipping method (Triani <i>et al.</i> , 2020)	9
Figure 2.2: Formation process of the aluminized layer during heat treatment process (Sun <i>et al.</i> , 2017).....	10
Figure 2.3: Back scattered SEM micrograph of (a) as-coated P91 and (b) as-coated 304 (Dorcheh and Galetz, 2016).....	13
Figure 2.4: SEM micrograph of Al slurry diffusion coatings after heat treatment of iron substrate in argon at 680°C (Montero <i>et al.</i> , 2017).....	14
Figure 2.5: Fe-Al binary phase diagram (Sina <i>et al.</i> , 2015).....	16
Figure 2.6: Variation of Gibbs free energy with temperature for Fe-Al intermetallic compounds (Yang <i>et al.</i> , 2018).....	17
Figure 2.7: Layer thickness versus the treatment time for temperature (a) 500°C and (b) 650°C (Triani <i>et al.</i> , 2020)	19
Figure 2.8: Layer thickness versus time graph of Mirrax ESR sample heat treated at 600, 650 and 700°C (Yener <i>et al.</i> , 2021).....	20
Figure 2.9: Variation in the thickness of aluminide layers produced at temperature 500°C and 650°C (Triani <i>et al.</i> , 2020).....	22
Figure 2.10: Inverse of the temperature (1/K) versus ln K (Triani <i>et al.</i> , 2020).....	23
Figure 2.11: Graph of (a) thickness versus time at 500°C, 550°C, 600°C and 650°C and (b) ln K in the function of 1/T (Troysi and Brito, 2020).....	24
Figure 2.12: Variation of the hardness of aluminides formed on the surface of Mirrax ESRsample (Yener <i>et al.</i> , 2021)	26
Figure 2.13: SEM micrograph of slurry aluminide coated T91 sample after 5000h at 650°C in 100% flowing steam (Hou <i>et al.</i> , 2020)	28
Figure 3.1: Slurry preparation using three different set of binders.....	35
Figure 3.2: Overall process flow of the project	36

Figure 3.3: Slurry-coated sample after deposition process.....	40
Figure 3.4: Slurry-coated sample placed in the crucible	40
Figure 3.5: Heat treatment profile of aluminide coated sample at 600°C, 630°C, 650°C, 680°C and 700°C for 4, 6, 8 and 10 hours.....	41
Figure 3.6: Scattered angle for large and small particles (Malvern Instruments Limited, 2013)	42
Figure 3.7: Sample mounted with epoxy resin and hardener in the PVC mould.	44
Figure 4.1: Particle size curve of aluminium particles	49
Figure 4.2: Particle size curve of alumina particles.....	49
Figure 4.3: SEM image of cross-section aluminide coating heated at 680°C for 4 hours for (a) test sample PVA, (b) test sample PVB, and (c) test sample PVB+2% AlCl ₃	51
Figure 4.4: (a) SEM image of cross-section and (b) EDX spectrum in the inner layer of aluminide coating for test sample PVA.....	52
Figure 4.5: (a) SEM image of cross-section and (b) EDX spectrum in the inner layer of aluminide coating for test sample PVB	52
Figure 4.6: (a) SEM image of cross-section and (b) EDX spectrum in the inner layer of aluminide coating for test sample PVB+2% AlCl ₃	52
Figure 4.7: XRD pattern of (i) test sample PVA, (ii) test sample PVB, and (iii) test sample PVB+2% AlCl ₃ after heat treatment at 680°C for 4 hours	54
Figure 4.8: Coating thickness of test sample PVA, PVB and PVB+2% AlCl ₃ after heat treatment at 680°C for 4 hours	55
Figure 4.9: SEM image of cross-section aluminide coating heat treated at 600°C for (a) 4 hours, and (b) 10 hours.....	58
Figure 4.10: SEM image of cross-section aluminide coating heat treated at 630°C for (a) 4 hours, (b) 8 hours and (c) 10 hours	59
Figure 4.11: (a) SEM image of cross-section and (b) EDX spectrum 1, 2, 3 and 4 of the aluminide coating and substrate heat treated at 630°C for 10 hours	60

Figure 4.12: (a) SEM image of cross-section, (b) FESEM cross-section image with horizontal line scan from topcoat to substrate, and (c) corresponding EDX concentration profile of sample heat treated at 630°C for 10 hours.....	61
Figure 4.13: SEM image of cross-section aluminide coating heat treated at 650°C for (a) 4 hours, (b) 6 hours, (c) 8 hours, and (d) 10 hours	62
Figure 4.14: (a) SEM image of cross-section and (b) EDX spectrum 1 in the aluminide coating heat treated at 650°C for 10 hours.....	63
Figure 4.15: (a) SEM image of cross-section and (b) EDX spectrum 2 in the aluminide coating heat treated at 650°C for 10 hours.....	63
Figure 4.16: (a) SEM image of cross-section and (b) EDX spectrum 3 in the aluminide coating heat treated at 650°C for 10 hours.....	64
Figure 4.17: (a) SEM image of cross-section and (b) EDX spectrum 4 in the substrate heat treated at 650°C for 10 hours	64
Figure 4.18: (a) SEM image of cross-section, (b) FESEM cross-section image with horizontal line scan from top coat to substrate and (c) corresponding EDX concentration profile of sample heat treated at 650°C for 10 hours.....	66
Figure 4.19: SEM image of cross-section aluminide coating heat treated at 680°C for (a) 4 hours, (b) 6 hours, (c) 8 hours, and (d) 10 hours	67
Figure 4.20: (a) SEM image of cross-section and (b) EDX spectrum 1 in the substrate heat treated at 680°C for 10 hours	68
Figure 4.21: (a) SEM image of cross-section and (b) EDX spectrum 2 in the substrate heat treated at 680°C for 10 hours	68
Figure 4.22: (a) SEM image of cross-section and (b) EDX spectrum 3 in the substrate heat treated at 680°C for 10 hours	68
Figure 4.23: (a) SEM image of cross-section and (b) EDX spectrum 4 in the substrate heat treated at 680°C for 10 hours	69

Figure 4.24: (a) SEM image of cross-section, (b) FESEM cross-section image with horizontal line scan from top coat to substrate, and (c) corresponding EDX concentration profile of sample heat treated at 680°C for 10 hours.....	71
Figure 4.25: SEM image of cross-section aluminide coating heat treated at 700°C for (a) 4 hours, (b) 6 hours, (c) 8 hours, and (d) 10 hours	72
Figure 4.26: XRD pattern of sample after heat treatment at 600°C for (i) 4 hours, and (ii) 10 hours.....	73
Figure 4.27: XRD pattern of sample after heat treatment at 630°C for (i) 4 hours, (ii) 8 hours, and (iii) 10 hours	74
Figure 4.28: XRD pattern of sample after heat treatment at 650°C for (i) 4 hours, (ii) 6 hours, (iii) 8 hours, and (iv) 10 hours	75
Figure 4.29: XRD pattern of sample after heat treatment at 680°C for (i) 4 hours, (ii) 6 hours, (iii) 8 hours, and (iv) 10 hours	76
Figure 4.30: XRD pattern of sample after heat treatment at 700°C for (i) 4 hours, (ii) 6 hours, (iii) 8 hours and (iv) 10 hours	77
Figure 4.31: (a) SEM image of cross-section of test sample 1 with entirely Al slurry composition, and (b) SEM image of cross-section of sample with 7Al : 3Al ₂ O ₃ slurry composition heat treated at 680°C for 4 hours.....	79
Figure 4.32: Coating thickness of sample after heat treatment at 650°C, 680°C and 700°C for 4, 6, 8 and 10 hours respectively	80
Figure 4.33: Thickness of FeAl layer of sample after heat treatment at 650°C, 680°C and 700°C for 4, 6, 8 and 10 hours respectively	81
Figure 4.34: Square of coating thickness of sample after heat treatment at 650°C, 680°C and 700°C for 4, 6, 8 and 10 hours respectively	82
Figure 4.35: ln K of the sample as a function of the inverse of the temperature at 650°C, 680°C and 700°C respectively	82

Figure 4.36: Square of thickness of FeAl of sample after heat treatment at 650°C, 680°C and 700°C for 4, 6, 8 and 10 hours respectively	83
Figure 4.37: ln K of FeAl of the sample as a function of the inverse of the temperature at 650°C, 680°C and 700°C respectively	83
Figure 4.38: Optical microstructure of the sample after heat treatment process	84
Figure 4.39: Area percentage porosity for sample after heat treatment at (a) 650°C (b) 680°C and (c) 700°C	85
Figure 4.40: SEM cross section image with label layer 1, 2, 3, 4 and 5 of sample heat treated at 700°C for 8 hours	86
Figure 4.41: Depth of penetration of 5 layer for sample after heat treatment at 700°C for 8 hours	88
Figure 4.42: Tafel plot for sample heat treated at 650°C, 680°C and 700°C for 8 hours and 10 hours	90

LIST OF SYMBOLS

°	Degree
°C	Degree Celsius
at.%	Atomic Percentage
wt.%	Weight Percentage
R	Gas Constant
Q	Activation Energy
K	Absolute Temperature
mm	Millimetre
µm	Micrometre
µm ²	Square Micrometre
nm	Nanometre
g	Gram
θ	Theta
ΔG	Gibbs Free Energy
ΔH	Enthalpy
mN	Milli Newton
V	Voltage
µA	Micro Ampere
D _v (50)	Mean Particle Size
D (4,3)	Mean Particle Size for Bimodal Distribution
h	Hours
s	Seconds
K ⁻¹	Inverse Kelvin

LIST OF ABBREVIATIONS

A-USC	Advanced Ultra-Supercritical
CFE	Cold-Field-Emission
CSP	Concentrated Solar Power
CTE	Coefficient Thermal Expansion
CVD	Chemical Vapour Deposition
EDX	Energy Dispersive X-ray
FESEM	Field Emission Scanning Electron Microscope
HTF	Heat Transfer Fluid
IDZ	Interdiffusion Zone
SEM	Scanning Electron Microscope
XRD	X-ray Diffraction

LIST OF APPENDICES

Appendix A	Measurement data on particle size of aluminium and alumina powder
Appendix B	Measurement data on aluminide coating thickness for test sample 1, 2 and 3 after heat treatment at 680°C for 4 hours
Appendix C	Measurement data on aluminide coating thickness for sample after heat treatment at 650°C for 4, 6, 8 and 10 hours
Appendix D	Measurement data on aluminide coating thickness for sample after heat treatment at 680°C for 4, 6, 8 and 10 hours
Appendix E	Measurement data on aluminide coating thickness for sample after heat treatment at 700°C for 4, 6, 8 and 10 hours
Appendix F	Measurement data on thickness of FeAl layer for sample after heat treatment at 650°C for 4, 6, 8 and 10 hours
Appendix G	Measurement data on thickness of FeAl layer for sample after heat treatment at 680°C for 4, 6, 8 and 10 hours
Appendix H	Measurement data on thickness of FeAl layer for sample after heat treatment at 700°C for 4, 6, 8 and 10 hours
Appendix I	Measurement data on area percentage porosity for sample after heat treatment at 650, 680 and 700°C for 8 and 10 hours
Appendix J	Measurement data on maximum depth for sample after heat treatment at 700°C for 8 hours
Appendix K	Measurement data on hardness for sample after heat treatment at 700°C for 8 hours
Appendix L	Measurement data on reduced modulus for sample after heat treatment at 700°C for 8 hours
Appendix M	Cross-sectional image of before and after indentation for sample after heat treatment at 700°C for 8 hours

MIKROSTRUKTUR DAN KINETIK PERTUMBUHAN SALUTAN ALUMINIDA PADA KELULI TAHAN KARAT 304 SECARA BUBURAN ALUMINISASI

ABSTRAK

Salutan aluminida melalui buburan aluminisasi telah menarik minat industri untuk meningkatkan rintangan kakisan bahan struktur yang beroperasi dalam persekitaran yang teruk. Namun, penyusutan aluminium daripada salutan ke dalam substrat dan ketidakpadanan dalam pekali pengembangan terma (PPT) menjadi halangan dalam membangunkan salutan aluminida pelindung yang baik. Keluli tahan karat austenit 304 telah dipilih sebagai substrat kerana ketidakpadanan PPT yang lebih kecil antara substrat dan salutan. Tambahan pula, Al_2O_3 ditambah kepada komposisi buburan sebagai agen aluminisasi untuk melambatkan resapan masuk aluminium ke dalam substrat. Matlamat projek ini adalah untuk mengkaji kesan suhu rawatan haba dan masa ke atas pembentukan salutan aluminida dengan kehadiran alumina. Sampel bersalut buburan telah dirawat haba pada pelbagai suhu (600, 630, 650, 680, dan 700°C) dan masa (4, 6, 8 dan 10 jam). Pada suhu 600 dan 630°C, terdapat lapisan nipis aluminida yang terbentuk kerana suhu rendah yang tidak dapat mendorong resapan keadaan-solid. Menurut analisis EDX, XRD dan kekerasan nano, FeAl_3 terbentuk di lapisan luar dan fasa FeAl dibangunkan dalam zon interdifusi (IDZ). Apabila suhu dan masa rawatan haba meningkat, ketebalan salutan aluminida dan ketebalan FeAl meningkat. Berdasarkan persamaan Arrhenius, tenaga pengaktifan untuk fasa FeAl_3 dan FeAl ialah 214.630 kJ/mol, manakala tenaga pengaktifan untuk fasa FeAl ialah 343.153 kJ/mol. Sampel yang dirawat haba pada 700°C selama 10 jam mempunyai rintangan kakisan yang lebih baik kerana ketebalan salutan yang lebih tebal. Salutan aluminida yang dibangunkan pada keluli tahan karat austenit 304 menghasilkan keputusan yang baik dan berpotensi digunakan sebagai pelindung salutan.

MICROSTRUCTURE AND KINETIC GROWTH OF ALUMINIDE COATING ON 304 STAINLESS STEEL BY SLURRY ALUMINIZING

ABSTRACT

Aluminide coating by slurry aluminizing has gained interest by industry to improve the corrosion resistance of structural materials operating in harsh environments. However, depletion of aluminium from the coating into the substrate and mismatch in coefficient thermal expansion (CTE) became obstacles in developing a good protective aluminide coating. Austenitic stainless steel 304 was chosen as the substrate due to the smaller CTE mismatch between substrate and the coating. Furthermore, Al_2O_3 was added to the slurry composition as an aluminizing agent to slow the inward diffusion of aluminium into the substrate. The aim of this project is to study the effect of heat treatment temperature and time on the aluminide coating formation with the present of alumina. The slurry coated sample was heat treated at various temperatures (600, 630, 650, 680, and 700°C) and times (4, 6, 8 and 10 hours). At 600 and 630°C, a thin layer of aluminide was formed due to the low temperature which not able to induce the solid-state diffusion. Based on EDX, XRD, and nano hardness analysis, FeAl_3 formed in the outer layer and FeAl phase developed in the interdiffusion zone (IDZ). The aluminide coating and FeAl thickness increase as heat treatment temperature and time increases. According to the Arrhenius equation, the activation energy for FeAl_3 and FeAl phase was 214.630 kJ/mol, while the activation energy for FeAl phase was 343.153 kJ/mol. Heat-treated samples at 700°C for 10 hours had better corrosion resistance due to thicker coating thickness. Aluminide coating developed on austenitic stainless steel 304 yields promising results and has the potential to be used as a protective coating.

CHAPTER 1

INTRODUCTION

1.1 Background

Austenitic 18-8-type stainless steels such as 304 stainless steel are the most commonly used materials in modern supercritical power plants due to its excellent properties against oxidation (Lu *et al.*, 2019). However, the limited oxidation resistance of these steels may result in deterioration of metal and might cause failure of material at high temperatures (Li *et al.*, 2017; Dorcheh and Galetz, 2016). Aluminide coatings showed an excellent oxidation resistance because of their ability to grow protective scales (Agüero *et al.*, 2018; Bates *et al.*, 2009; Lu *et al.*, 2021). Thus, attempts using aluminide coatings to improve the oxidation resistance of boiler tube steels, turbine blade and concentrated solar power (CSP) have been made by means of various methods, such as chemical vapour deposition (CVD), pack aluminizing and slurry aluminizing. Slurry aluminizing has been increasingly gained interest in aluminizing large parts because it is the easier to manufacture, environmentally friendly process and low cost. Aluminide coating by slurry route is performed by spraying or painting the aluminium slurry on the surface of substrate and followed by a heat treatment process in an inert environment to produce an aluminide diffusion layer. The diffusion coating contained intermetallic compound that acts as a reservoir phase (Montero *et al.*, 2015; Dorcheh and Galetz, 2016). Aluminide coatings exhibited outstanding corrosion protection against steam oxidation and corrosive environment because of their capability to grow alumina protective scales (Agüero *et al.*, 2018; Bates *et al.*, 2009; Lu *et al.*, 2021).

Aluminide coating is composed of intermetallic compounds formed between iron and aluminium (Troysi and Brito, 2020). There are five types of intermetallic compounds formed in aluminide coating such as Fe_2Al_5 , FeAl_3 , FeAl_2 , FeAl and Fe_3Al (Kobayashi

and Yakou, 2002). Researchers found that the phase of Fe_2Al_5 is preferable to be formed due to the smallest Gibbs free energy and followed by the phase of FeAl_3 , FeAl_2 and FeAl . The phase of Fe_3Al is not formed because the Gibbs free energy is greater than zero when the temperature is above than 400°C (Dong *et al.*, 2019). The aluminide coating can serve as a protective layer to the substrate because the coatings can form an alumina scale in high temperature (Agüero *et al.*, 2008). Lu et al. (2019) testified that the aluminide coating formed on Super304H steel has greatly increase the oxidation resistance where a thin alumina scale was developed when exposed to high steam temperature at 650°C for 1000 h. Triani et al. (2020) observed that the aluminide coating formed on the AISI 304 stainless steel had good thickness uniformity with well-defined interface with the substrates.

The formation of aluminide layers are affected by some parameters such as the reactivity of aluminium in the powder and on the substrate, influence of the heat treatment atmosphere and particle size (Triani *et al.*, 2020). It is challenging to obtain a good protective aluminide coating as the process involve complex chemical reactions. Therefore, the development of aluminide coating on substrate is crucial to ensure that the coating contains the phases required which are FeAl and Fe_3Al to withstand high corrosive and oxidation environment.

1.2 Problem Statement

Aluminide coating exhibit excellent oxidation resistance because the intermetallic compound of Fe-Al can form a thin layer of alumina film on the coating surface when expose to a high temperature oxidation environment. The phases of FeAl and Fe_3Al is required due to oxidation resistance at high temperature and also provide good bonding between coating and substrate. However, the main problems are depletion of aluminium

from the coating into the substrate alloy and coefficient of thermal expansion (CTE) mismatch. Depletion of aluminium due to the inward diffusion of aluminium into substrate alloy had resulted the formation of rich Al precipitates and voids. The formation of aluminium-rich brittle intermetallic compounds such as Fe_2Al_5 and FeAl_3 had greatly increased the rate of corrosion. Austenitic steels were chosen because CTE value of austenitic steels is $\sim 18 \times 10^{-6} \text{ K}^{-1}$ at 650°C which has a smaller CTE mismatch to the coating which is $\sim 17 \times 10^{-6} \text{ K}^{-1}$ at 650°C . Thus, cracking in the coating may reduce when used of austenitic stainless steel as the substrate. The depletion of aluminium and formation of different intermetallic compound are influenced by the composition of the aluminizing agent, aluminizing temperature and time. Al_2O_3 particles as aluminizing agent (inert filler material) was added into slurry composition to slow down the inward diffusion of aluminium into substrate. Al_2O_3 particles was added into slurry composition to slow down the inward diffusion of aluminium into substrate. Al_2O_3 will limit the availability of aluminium present to diffuse into stainless-steel substrate by absorbing the heat available, leaving less heat available for aluminium to melt. Thus, the activity of aluminium was reduced, slowing down the diffusion of Al into substrate and avoid the formation of Al-rich intermetallic compounds. Furthermore, adding Al_2O_3 may also lower the depletion loss of Al from coating to substrate via interdiffusion, improving coating layer by forming solid solution (Javan et al., 2019). The diffusion of aluminium depends on temperatures and times and the present of alumina filler material. Although some research has been done using alumina, other factors such as temperature and time may have an impact on the mechanism and growth kinetics of aluminide coating formation. Thus, it is necessary to investigate the effect of temperature and time on formation of aluminide coating with the present of alumina.

1.3 Objective

The objectives of this project are as follows:

1. To investigate the effect heat treatment temperatures and times on the formation of aluminide coating with alumina addition.
2. To evaluate the surface morphology, chemical composition, and phase of the aluminide coating.
3. To determine the growth kinetics, hardness, and corrosion behaviour of the aluminide coating.

1.4 Thesis Outline

This thesis was divided into five chapters. Chapter 1 gives a brief overview of the project study background as well as problem statement and objectives for this project. Meanwhile, Chapter 2 is literature review which covered the austenitic stainless steel, aluminide coating, general applications of aluminide coating and slurry aluminizing process. In addition, effect of the temperature and time on the aluminide coating, growth kinetics of the aluminide layer, hardness as well as corrosion behaviour of the aluminide coating were discussed in this chapter. Chapter 3 describes the raw materials used as well as methodologies for sample preparation, slurry preparation, sample preparation for mounting and characterization technique used in this project. The experimental results and data were analysed and interpreted in Chapter 4. A detail discussion about the surface morphology, phase, and growth kinetics were discussed in this chapter. Last but not least, Chapter 5 summarized the research finding and recommendations were made for future work.

CHAPTER 2

LITERATURE REVIEW

2.1 Introduction

In this chapter, the background of austenitic stainless steel, aluminide coating, slurry aluminizing technique, general application of aluminide coating, slurry aluminizing process, effect of temperature and time on aluminide coating, growth kinetic, hardness and corrosion behaviour of aluminide coating of previous studies were discussed in detail.

2.2 Austenitic stainless steel

Stainless steels are high alloy steels that very resistant to corrosion in a variety of environments. Chromium is the predominant alloying element in the stainless steel, and it is required concentration at least of 11 wt.% chromium content. Other alloying elements such as nickel and molybdenum are added to improve the corrosion resistance. Stainless steel can be categorized into three classes based on the predominant phase constituent of the microstructure which are martensitic, ferritic and austenitic (Callister and Rethwisch, 2014).

Austenitic stainless steels are the most corrosion resistant due to its high content of chromium and also addition of nickel. Moreover, austenitic stainless steel can be hardened and strengthened by cold-work and it is non-magnetic (Callister and Rethwisch, 2014). Thus, austenitic stainless steels are commonly used in various applications that are required service at high temperature environment such as concentrated solar power (CSP).

Stainless steel 304 is used in this project and it is also known as 18-8-type austenitic stainless steel. It has the chromium and nickel content of approximately 18

wt.% and 8 wt.% respectively. It is typically used in ultra-supercritical power plants that required to withstand steam temperatures up to 650°C. Although stainless steel 304 exhibit high corrosion resistance, high creep strength and excellent welding performance, it can be corroded easily once the steam temperature above 620°C. The rate of corrosion is increased via the formation of undesirable thick Fe-containing oxide scale with increasing temperature (Lu *et al.*, 2019, 2021). Lu *et al.* (2019) reported that austenitic alloy such as Super304H that used in boilers will grow a double layered oxide scales that consisted of an Fe₃O₄ outer layer and Fe-Cr-O spinel inner layer when exposed to a high temperature.

Moreover, the sensitization of the stainless steel may happen when it is heated in between 550°C and 800°C. The corrosion resistance of these steels will be degraded due to the chromium carbides precipitates at the grain boundaries (Triani *et al.*, 2020). There is lack of chromium in the interior of the grains to form the chromium oxide and cause the steel to corrode rapidly (Askeland *et al.*, 2010).

The use of these alloys in CSP application is also limited by the corrosion resistance because the steels are directly contact with molten salt. Dorcheh and Galetz (2016) reported that high chromium austenitic steels (304 and 316) have lower corrosion rates in molten salt compared to the low chromium steels. This is because corrosion protection is provided through the formation of a continuous layer of chromium oxide. However, chromium can be soluble when in contact with molten salt and thus inhibiting the protective oxide layer formation. As a result, corrosion of steels can be occurred as the protective layer cannot be formed due to the interaction with the molten salts at high temperature (Agüero *et al.*, 2018).

The corrosion resistance of stainless steel 304 is limited when involve the molten salt at high temperature such as CSP. To solve this issue, aluminide coating has been

introduced to modify the surface of the stainless steel 304 in order to increase the service life in high temperature environments. Few studies have been done to investigate the corrosion resistance of the aluminide coating formation on the austenitic stainless steel (Agüero *et al.*, 2008; Lu *et al.*, 2019; Dorcheh and Galetz, 2016; Z. Yang *et al.*, 2020).

2.3 Aluminide coating

Aluminide coating is widely used to reduce the effect of oxidation and corrosion of the substrate at higher temperature applications. Aluminide coating can be produced by applying aluminium on the surface of iron-based alloys and a thin layer of iron-aluminide intermetallic compounds will be formed. It can serve as a protective layer to the substrate because the coatings can form an alumina scale in a steam temperature (Agüero *et al.*, 2008).

Lu *et al.* (2019) testified that the aluminide coating formed on Super304H steel has greatly increase the oxidation resistance where a thin alumina scale was developed when exposed to high steam temperature at 650°C for 1000 h. Dorcheh and Galetz (2016) reported that aluminized ferritic-martensitic P91 and austenitic 304 in molten nitrate salts at 600°C have better corrosion resistance compared to un-coated P91 and 304 alloys.

Triani *et al.* (2020) observed that the coating formed on the AISI 304 stainless steel had good thickness uniformity with well-defined interface with the substrates. The same result is obtained after heat treated at 500°C and 650°C. The FeAl phase formed on the coating is confirmed by using X-ray diffraction for both heat treatment temperature.

Other than that, Super304H steel that carried out aluminizing process at 980°C for 0.5 h had developed a double layer structure and there is no through-crack observed. Based on XRD analysis, a single phase of β -FeAl was identified as the major phase in the

as-deposited coating (Lu *et al.*, 2021). Thus, the aluminide coating can act as a protective layer to the substrate against the attack from corrosion.

2.4 Aluminide coating technique - Slurry Aluminizing

In this project, slurry aluminizing technique is used to develop the aluminide coating on the substrate surface. Slurry aluminizing process is carried out by preparing the aluminium-containing slurry and coated onto the surface of prepared sample and dried it before heat treatment process. Aluminide layer will be formed during heat treatment which the slurry applied on the surface will react with the substrate (Montero *et al.*, 2017). Slurry aluminizing method is simple and has been studied by several researchers. Slurry aluminizing can be performed by three ways: dipping, spraying, and brushing technique.

Triani *et al.* (2020) applied slurry aluminizing by dipping process to deposit the slurry on the surface of AISI 304 stainless steel whereas Lu *et al.* (2021), Lu *et al.* (2019) and Montero *et al.* (2017) deposited the aluminium-slurry by air spraying on the surface of substrate. Huang *et al.* (2019) also sprayed the slurry uniformly to a thickness around 0.05 mm on the TP347H FG austenitic stainless steel. Moreover, the slurries were homogenized by magnetic stirring before spraying process carried out (Agüero *et al.*, 2018). Figure 2.1 shows the slurry aluminization steps by dipping method.

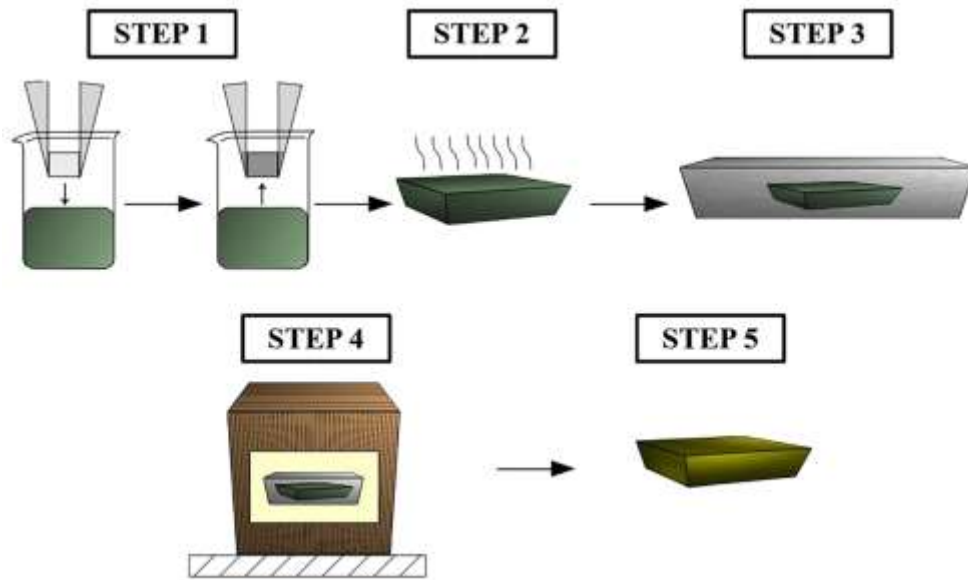


Figure 2.1: Slurry aluminization steps by dipping method (Triani *et al.*, 2020)

Besides aluminizing by spraying and dipping, Dorcheh and Galetz (2016) used airbrush technique to deposit the slurry onto the surface of ferritic-martensitic steel P91 and stainless steel 304. Similarly, Kepa *et al.* (2020) also sprayed the slurry by an airbrush method on the pure nickel samples and pure Armco iron samples. Agüero *et al.* (2008) deposited the Al slurry on the ferritic steel P92 using brush or spray gun technique. In contrast, Sun *et al.* (2017) and Dong *et al.* (2019) produced the aluminide coating on 316L stainless steel by applying the combined method of surface slurry pre-coating and low temperature aluminizing technique. Figure 2.2 indicates the formation process of aluminized layer.

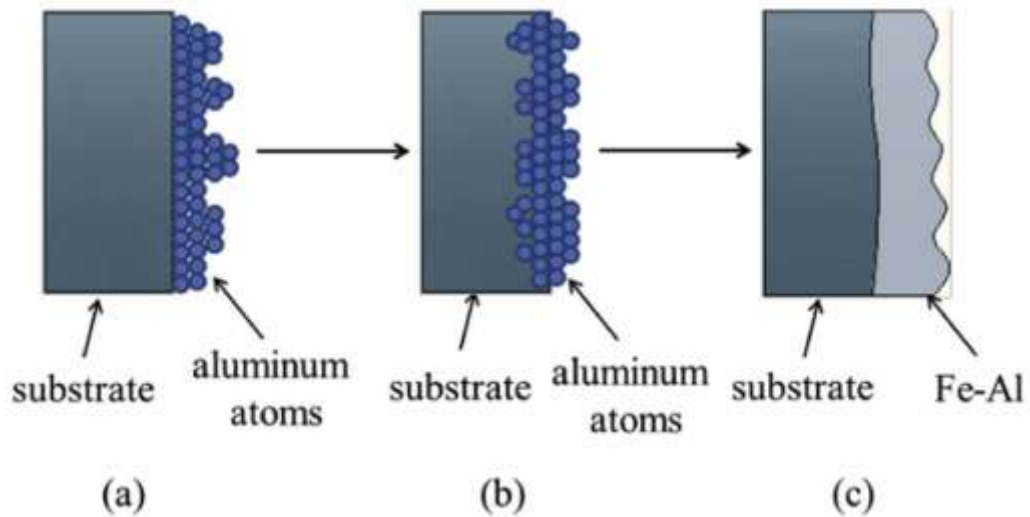


Figure 2.2: Formation process of the aluminized layer during heat treatment process (Sun *et al.*, 2017)

2.5 General applications of aluminide coating

The development of aluminide coating had been applied extensively to protect the structural materials that are used for the high temperature applications or complex chemical environments. Aluminide coating are commonly used to extend the operating lifespan of the components by developing a protective oxide scale such as Al_2O_3 on the surface of substrate at operating temperature (Leng *et al.*, 2020; Taylor and Patnaik, 2007).

Concentrated solar power (CSP) is a major renewable energy technology that can provide clean electricity and continuous power systems by using an unlimited source of energy (the sun) nowadays. The use of molten nitrate salts as the heat transfer fluid (HTF) inside the receiver tank required to keep the temperature above the freezing point of the molten salt ($\sim 225^\circ\text{C}$) in order to maintain the power cycle. CSP is very expensive, and one way to cut costs is to increase the efficiency of the steam turbine by raising the steam temperature and pressure. However, this will induce the corrosion problem of the storage tanks and piping in the CSP systems that operated at such corrosive environment. Hence,

iron aluminides were introduced to act as the resistant materials to protect the structural materials for application that operated at aggressive environment. Aluminide coating on the surface of substrate can reduce the rate of corrosion by producing alumina scale in molten nitrate salt environment (Audigié *et al.*, 2017; Oskay *et al.*, 2019; Dorcheh and Galetz, 2016).

Besides CSP applications, aluminide coating also can be applied on the ferritic-martensitic steel that used in the advanced ultra-supercritical (A-USC) boiler applications. Advanced ultra-supercritical (A-USC) boiler is a technology that can be used for the development of a coal-fired power plant. This technology worked at temperature around 650°C to 720°C with steam pressure of 25 MPa to 35 MPa. The high working temperature and steam pressure of A-USC boiler as well as the fly ash produced by coal combustion which contained of alkali oxides had accelerated the degradation of the material in the boiler construction. Aluminizing process was carried out on the ferritic-martensitic steel and the formation of iron aluminide coating had improved greatly the performance of the steel in the boiler applications (Liang and Wang, 2019). In addition, Lu *et al.*, (2019) also studied the performance of aluminized Super 304H steel that used in the USC boiler tube. Their study proved that aluminizing process helped to increase the corrosion resistance of the sample with a steam temperature at 650°C in the USC boiler application.

Moreover, another application of the intermetallic coating is in the gas turbine industry area. It usually used to protect turbine blade and nozzle guide vanes from high temperature oxidation and hot corrosion environment. The hot end of the compressor along with a conversion top coat was coated by these iron aluminides. This is because the layer will give anodic sacrificial protection to the surface of steel whereas the conversion top coat provided a hard sealant-type surface that can avoid premature corrosion of the

aluminide coating when exposed to the application environment. Other than that, applications such as chemical plant heat exchangers, petroleum refining and tail gas treatment equipment which worked at high temperature also required aluminide coating to improve the oxidation resistance of the components (Taylor and Patnaik, 2007).

2.6 Slurry aluminizing process

In slurry aluminizing method, slurry composition is one of the important parameters in determining the quality and microstructure of aluminide coating (Agüero *et al.*, 2008). Slurry is a mixture that are consisted of a binder and powder mixture. Different slurry composition can be prepared to produce the aluminide coating on the substrate surface. Many researchers had performed slurry aluminizing process using slurry that are produced using different slurry composition.

Kepa *et al.* (2020) studied the formation of aluminide coating by using fast aluminizing and conventional aluminizing method. A 57 wt.% of binder mixture of polyvinyl alcohol (PVA) and water in the mass ratio of 1:10 and 43 wt.% of aluminium powder were used to form the slurry. An air brushed was used to spray a thick slurry on one side of the sample while a thin slurry was deposited on the other side. In fast aluminizing, the deposited substrate is heated at 1080°C with heating rate of 100°C/min for 5 minutes. Three distinct layers are formed in thick deposits which are FeAl₂, FeAl and Fe(Al) whereas thin deposits produced two layered on the substrate which consisted of FeAl and Fe(Al). In contrast, Fe(Al) is formed on the most of the coating in conventional heat treatment which is heated at 1080°C for 2 hours with 25°C/min, 100°C/min and 5 hours with 100°C/min for thick and thin deposit. However, FeAl is generated on the thick coating when heated at 1080°C for 2 hours with heating rate of 100°C/min.

Dorcheh and Galetz (2016) used the slurry composed of aluminium powder mixed with polyvinyl alcohol and distilled water. An aluminide coating consisted of Fe_2Al_5 in the outer layer and a thinner FeAl layer in the inner layer were developed in P91 ferritic and 304SS sample. Figure 2.3 shows the back scattered scanning electron microscope (SEM) micrograph of as-coated P91 and as-coated 304 sample.

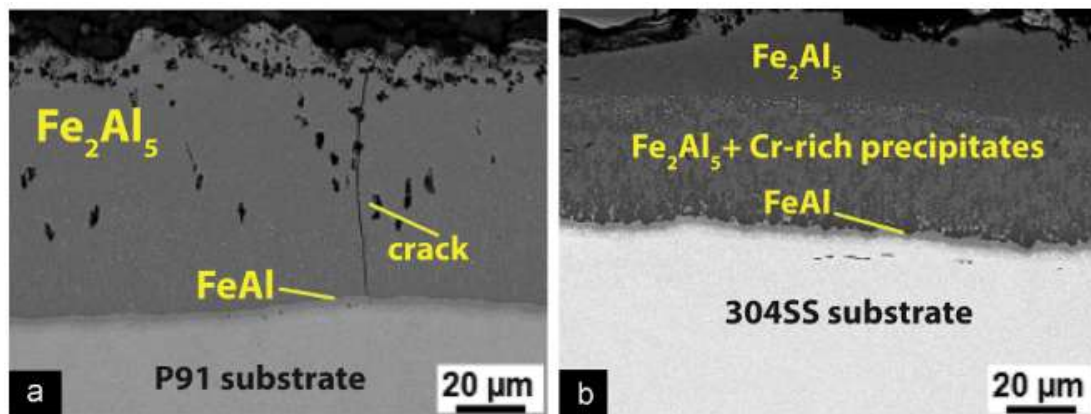


Figure 2.3: Back scattered SEM micrograph of (a) as-coated P91 and (b) as-coated 304 (Dorcheh and Galetz, 2016)

Similarly, Montero *et al.* (2017) used water-based slurry with polyvinyl alcohol in 10:1 mass ratio mixed with aluminium in the mass ratio of 1.3:1 to prepare slurry mixture. The air sprayed deposited slurry on the samples was then heated at 680°C for 2h in the heating rate between 1 and $10^\circ\text{C}/\text{min}$. An aluminide coating layer was formed on the iron substrate after aluminizing process. Fe_2Al_5 was formed and the composition changed to FeAl closer to the sample. Figure 2.4 shows SEM micrograph of Al slurry diffusion coatings after heat treatment of iron substrate in argon at 680°C .

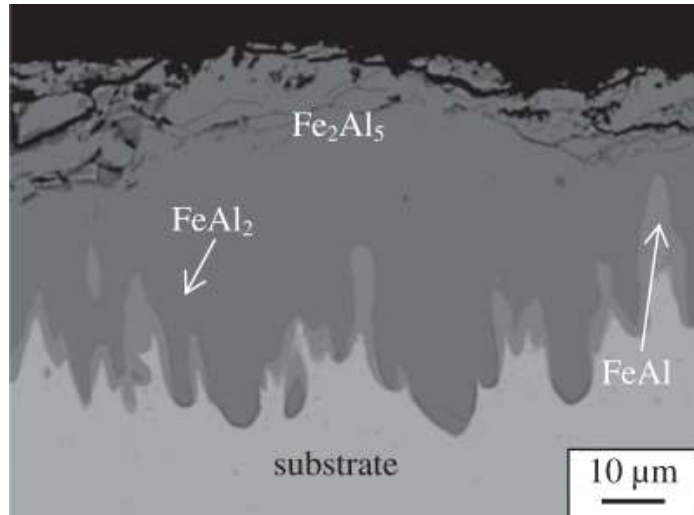


Figure 2.4: SEM micrograph of Al slurry diffusion coatings after heat treatment of iron substrate in argon at 680°C (Montero *et al.*, 2017)

Besides, Lu *et al.* (2019) and Lu *et al.* (2021) prepared slurry mixture that contained of 20 wt.% Al, 10 wt.% Si, 25 wt.% Al₂O₃ and 45 wt.% phosphate solution. A single phase of β -FeAl was detected in the coating after aluminizing process.

The formation of aluminide coating on stainless steel 304 by slurry route also studied by Triani *et al.* (2020). Other than using PVA and distilled water, slurry composition consists of mixture of 10 wt.% Al, 2 wt.% AlCl₃ as an activator and 88 wt.% Al₂O₃ as an inert compound while polyvinyl butyral (PVB) was used as the binder in the 2:1 mass ratio of powder mixture and PVB. Ethyl alcohol was added to produce the slightly viscous mixture. Dipping process was carried out to deposit the slurry on the samples and dried for 15 minutes in the air. The samples were then heat treated at 500°C and 650°C for 2, 4, 6, and 8 hours. A well-defined FeAl layer with good thickness uniformly was formed on the substrates.

In addition, Sun *et al.* (2017) prepared 2.7g of PVB as a binder in 55g of solvent ethanol with mass ratio of 1:20 and 10g of powder mixture composed of 86 wt.% Al, 5 wt.% Ce₂O₃ and 9 wt.% Cr was added to prepare pre-coating slurry. After surface slurry pre-coating, the 316L stainless steel samples were aluminized by using powder embedded

aluminizing method where the powder mixture composed of 30 wt.% Al, 65 wt.% Al₂O₃ and 5 wt.% AlCl₃. The aluminide coating produced a fine and regular grains with some pits on the substrate surface and it has a thickness around 50 μm.

Other than different slurry composition, particle size of aluminium powder and alumina powder on the microstructural of aluminide coating were studied by Javan *et al.* (2019). The author used three different particle size of Al with size of 250, 20 and 3 μm while fixed the particle size of Al₂O₃ (44 μm). Nickel-based superalloy (IN738LC) was the substrate material and pack cementation process were conducted at 750°C for 4h to form the aluminide coating. The analysis showed that the thickness is getting lower with decreasing particle size of aluminium. This might due to the smaller particle size of aluminium to the alumina particles had a negatively effect on the aluminium activity during aluminizing process as alumina particles can reduce the local melting of aluminium particles.

2.7 Effect of temperature and time on aluminide coating

In this project, the processing parameter such as temperature and time were varied accordingly to investigate the thickness of aluminide coating formation. Temperature plays an important role to determine the phases of aluminide layer because different intermetallic compounds may be formed as illustrated in Figure 2.5.

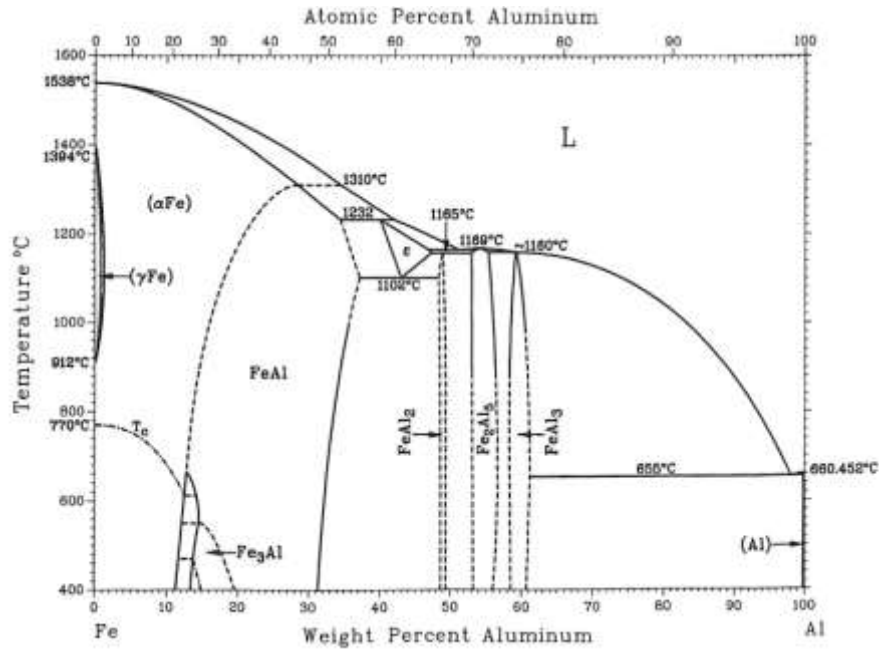


Figure 2.5: Fe-Al binary phase diagram (Sina et al., 2015)

According to the Fe-Al phase diagram and Gibbs free energy of iron-aluminide intermetallic compound, different chemical reactions between the interdiffusion of Fe and Al that are possible to occur during aluminizing process are shown in Table 2.1. Table 2.2 shows the Gibbs free energy for intermetallic compounds at temperature of 600°C, 630°C, 650°C, 680°C and 700°C.

Table 2.1: Different intermetallic compound and its Gibbs free energy (Dong *et al.*, 2019; Y. Yang *et al.*, 2018)

Intermetallic compound	Gibbs free energy, ΔG (kJ/mol)
$\text{Fe} + 5\text{Al} \longrightarrow \text{Fe}_2\text{Al}_5$	$\Delta G = -201636 + 42.56 T$
$\text{Fe}_2\text{Al}_5 + \text{Al} \longrightarrow 2\text{FeAl}_3$	$\Delta G = -111368 + 16.95 T$
$\text{Fe} + 2\text{Al} \longrightarrow \text{FeAl}_2$	$\Delta G = -81642 + 10.82T$
$\text{Fe}_2\text{Al}_5 + 3\text{Fe} \longrightarrow 5\text{FeAl}$	$\Delta G = -48483 + 4.88 T$
$3\text{Fe} + \text{Al} \longrightarrow \text{Fe}_3\text{Al}$	$\Delta G = -57192 + 82.28 T$

Table 2.2: Gibbs free energy for intermetallic compounds at temperature of 600°C, 630°C, 650°C, 680°C and 700°C

Intermetallic compound	ΔG , (kJ/mol) at T = 600°C	ΔG , (kJ/mol) at T = 630°C	ΔG , (kJ/mol) at T = 650°C	ΔG , (kJ/mol) at T = 680°C	ΔG , (kJ/mol) at T = 700°C
Fe₂Al₅	-164.48	-163.20	-162.35	-161.08	-160.23
FeAl₃	-96.57	-96.06	-95.72	-95.21	-94.88
FeAl₂	-72.20	-71.87	-71.66	-71.33	-71.11
FeAl	-44.22	-44.08	-43.98	-43.83	-43.73
Fe₃Al	14.64	17.11	18.75	21.22	22.87

Figure 2.6 illustrates the variations of Gibbs free energy with temperature for iron-aluminide intermetallic compounds.

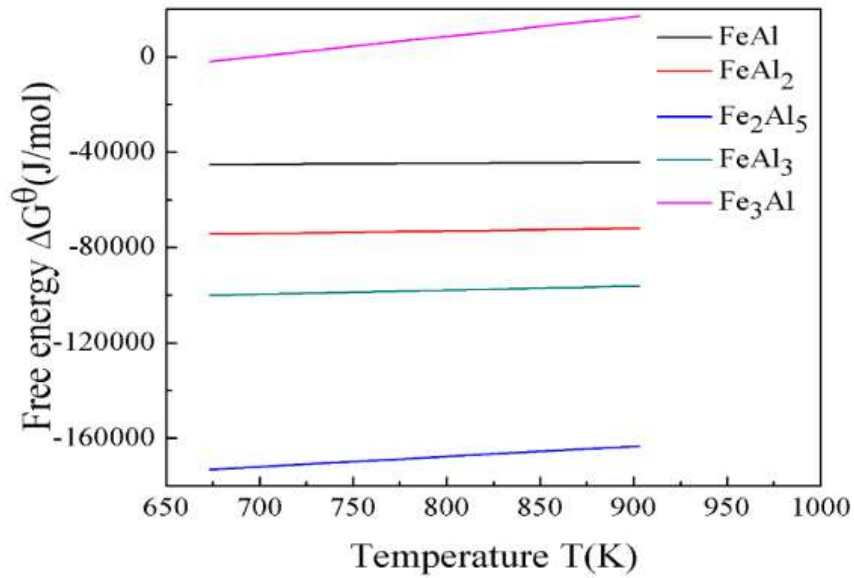


Figure 2.6: Variation of Gibbs free energy with temperature for Fe-Al intermetallic compounds (Yang *et al.*, 2018)

Based on the table and figure above, it is indicated that the Fe₂Al₅ will be formed first due to the lowest Gibbs free energy. Yang *et al.* (2018) found that the possible formation order of Fe-Al intermetallic compounds is Fe₂Al₅ > FeAl₃ > FeAl₂ > FeAl

according to the thermodynamic calculation as shown in Table 2.1. FeAl_2 phase is metastable and thus it will not be formed although it has a negative Gibbs free energy value (Dong *et al.*, 2019). Owing to the positive value of Gibbs energy for Fe_3Al at temperature of 600°C , 630°C , 650°C , 680°C and 700°C , it is indicated that Fe_3Al phase cannot be formed. However, this phase will begin to form when the temperature is cooled down to below 422°C due to the negative Gibbs free energy (Dong *et al.*, 2019).

Dong *et al.* (2019) observed that the coating become continuous with increasing heat treatment temperature and time. The coating consisted of Fe_2Al_5 and FeAl_3 phases at 600°C for 2 hours and the phases are converted to a single Fe_2Al_5 when prolong the aluminizing time to 3 and 4 hours. In contrast, four phases which are Fe_2Al_5 , FeAl_3 , FeAl and Fe_3Al are all observed at heat treatment temperature of 650°C and 680°C . Besides, they also reported that the coating thickness is increasing with the aluminizing temperature and time from 600°C to 680°C and from 2 hours to 4 hours respectively. The increased in the heat treatment temperature and time will drive in diffusion process for aluminide layer formation.

Besides, Triani *et al.* (2020) also found that the coating thickness is increased with the treatment time and temperature and the diffusion coefficient is higher when the temperature is at 650°C compared to the temperature at 500°C . This showed that the growth kinetic of aluminide layer is increasing with the temperature and time. Figure 2.7 shows the layer thickness versus the treatment time for temperature 500°C and 650°C .

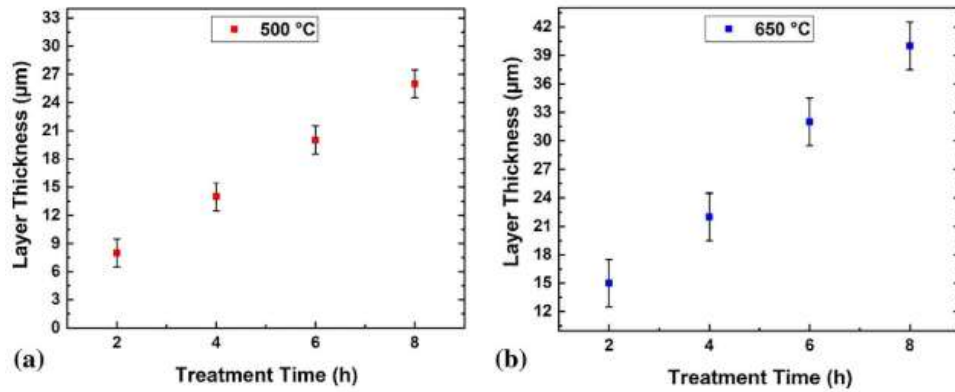


Figure 2.7: Layer thickness versus the treatment time for temperature (a) 500°C and (b) 650°C (Triani *et al.*, 2020)

In addition, Yener *et al.* (2021) also studied the thickness layer of the aluminide coating developed on the Mirrax ESR steel using low-temperature aluminizing process. It is observed that the coating thickness is increased with increasing heat treatment temperature and time as indicated in Figure 2.8. Figure 2.8 shows the layer thickness versus time graph of Mirrax ESR sample heat treated at 600, 650 and 700°C. A very thin and porous with 1-2 µm thick layer was formed at 600°C for 4h and the coating became more intense and glossy appearance with increasing temperature to 650°C and 700°C. Moreover, the rapidly increase in the coating thickness was also observed with increasing time from 4 to 6h. With an aluminizing temperature of 700°C for 6 hours, the coating thickness was found to be 45-50 µm.

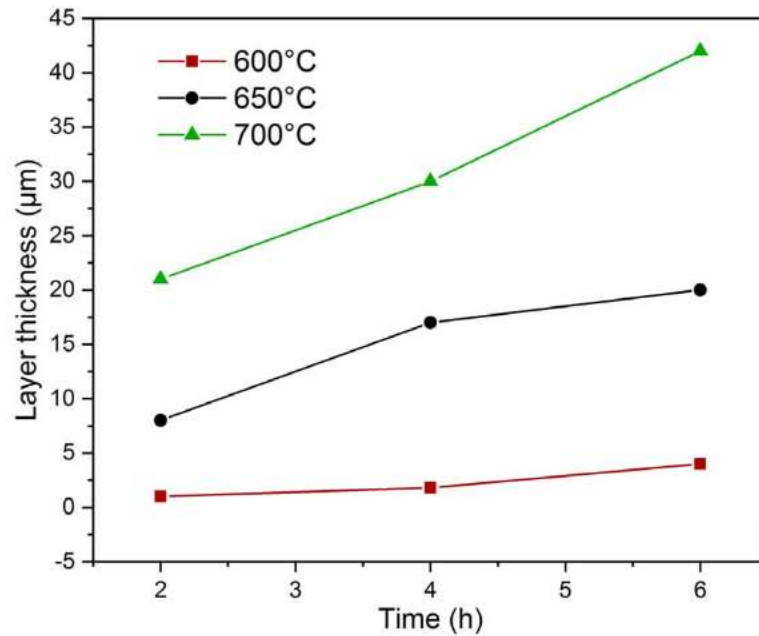


Figure 2.8: Layer thickness versus time graph of Mirrax ESR sample heat treated at 600, 650 and 700°C (Yener *et al.*, 2021)

2.8 Growth kinetic of aluminide coating

Growth kinetic of aluminide coating are influenced by the temperature and time of the aluminizing process. During the process, the magnitude of the diffusion coefficient of Al in the iron-aluminium phase is larger than the Fe. Thus, the growth activation energy of the aluminide coating can be expressed by the activation energy of Al in the iron-aluminium phase (Dong *et al.*, 2019). There are several studies shown that the formation of aluminide layer follows the parabolic law equation 2.1 (Dong *et al.*, 2019; Triani *et al.*, 2020; Zarei *et al.*, 2020):

$$X^2 = Kt \quad (\text{equation 2.1})$$

where X stands for the thickness of aluminide layer, K represents the growth rate constant and t is the aluminizing time of slurry.

Growth rate constant or diffusion coefficient (K) also can be determined by using Arrhenius equation 2.2. This equation shown the relationship of activation energy (Q) and the temperature (T) in Kelvin to the diffusion coefficient (K).

$$K = K_0 \exp\left(\frac{-Q}{RT}\right) \quad (\text{equation 2.2})$$

where K_0 refers to the pre-exponential constant, Q represents activation energy, T indicates absolute temperature and R is the gas constant.

The pre-exponential constant, K_0 provides a measure of the frequency of occurrence of the reaction situation which is commonly envisaged as incorporating the vibration frequency in the reaction coordinate. In contrast, activation energy, Q is defined as the energy barrier that must be overcome to allow the occurrence of the bond redistribution steps needed to convert reactant into products (Galwey and Brown, 1995). The absolute temperature in Kelvin is referred to the slurry aluminizing temperature whereas the value of gas constant is $8.314 \text{ J mol}^{-1} \text{ K}^{-1}$. Equation 2.2 can be further expressed in a linear relationship as shown in equation 2.3. From the growth rate constant, the activation energy (Q) of the aluminide coating prepared by different temperatures and times are determined by using equation 2.3.

$$\ln K = (\ln K_0) - \frac{Q}{RT} \quad (\text{equation 2.3})$$

Table 2.3 indicates the enthalpies formation and activation energies for growth of various Fe-Al intermetallic phases. Based on Table 2.3, Fe_2Al_5 and FeAl_3 had a more negative enthalpy value than FeAl and Fe_3Al intermetallic phases. Therefore, driving force is much larger to form Fe_2Al_5 and FeAl_3 intermetallic phases compared to other phases. At the same time, the activation energy for Fe_2Al_5 layer to grow is lower than others iron aluminide phases. Hence, the formation and growth of aluminium rich intermetallic layer Fe_2Al_5 and FeAl_3 are more favoured based on enthalpy and activation energy value.

Table 2.3: Enthalpies of formation and activation energies for growth of various Fe-Al intermetallic phases (Dangi *et al.*, 2018)

Intermetallic phases	ΔH_{298} (kJ/mol)	Activation energy (kJ/mol) (700-900°C)
FeAl	-51.24	180
Fe ₃ Al	-57.37	260
Fe ₂ Al ₅	-194.04	74.1
FeAl ₃	-112.56	Not reported

Triani *et al.*, (2020) studied the growth kinetics of iron aluminide layers produced on the AISI 304 stainless steel by slurry aluminizing using the equation 2.1 and equation 2.3. Figure 2.9 shows the variation in the thickness of the layers produced at temperature 500°C and 650°C calculated based on equation 2.1.

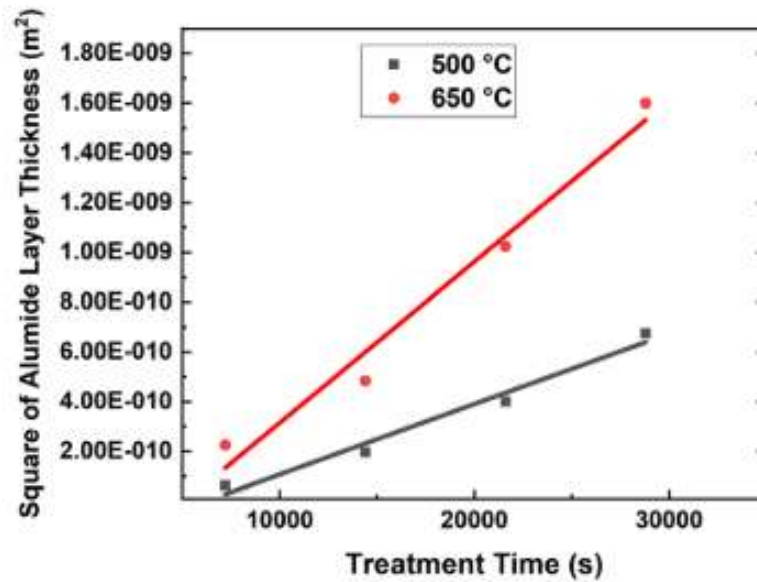


Figure 2.9: Variation in the thickness of aluminide layers produced at temperature 500°C and 650°C (Triani *et al.*, 2020)

From Figure 2.9, diffusion coefficient (K) at temperature 500°C and 650°C were obtained from the slope of the lines with the values of 2.87×10^{-14} m²/s and 6.576×10^{-14} m²/s respectively. After that, the value of ln K were calculated by using equation

2.3 and a graph of inverse of the temperature ($1/K$) versus $\ln K$ determined were plotted as shown in Figure 2.10.

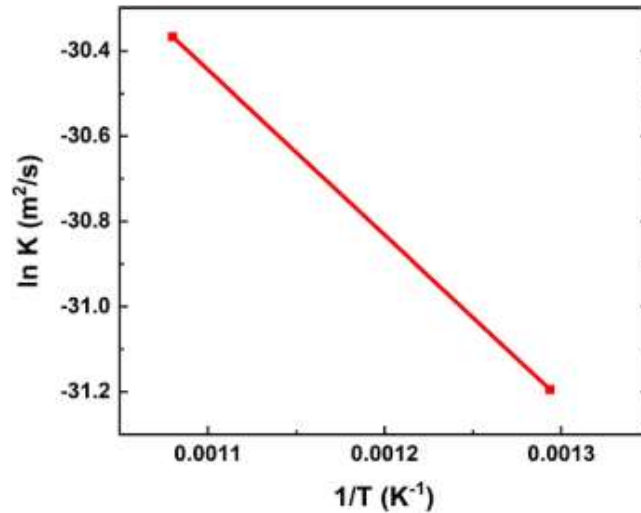


Figure 2.10: Inverse of the temperature ($1/K$) versus $\ln K$ (Triani *et al.*, 2020)

Based on Figure 2.10, the activation energy (Q) was obtained from the slope as it is represented as $-Q/R$ as mentioned in equation 2.3. The activation energy was determined as 34.5 kJ/mol. The pre-exponential constant (K_0) was found to be 6.09×10^{-12} m²/s by using the value of activation energy and diffusion coefficient.

Xiang and Datta (2006) studied the growth kinetics of aluminide coating that produced using pack cementation. From the result, they found that heat treatment time and temperature will influence only on thickness but not on the phases formation. The result showed that the aluminium concentration at outer layer achieve a constant value in 1 hour for all processing parameter and its concentration is decreased sharply at the interface between substrate and coating.

Dong *et al.* (2019) reported aluminde coating formed on the 316L stainless steel at different temperatures (600°C, 650°C and 680°C) for 2 hours, 3 hours and 4 hours. The diffusion coefficient at 600°C, 650°C and 680°C were determined and $\ln K$ were calculated as -30.25 ± 0.02 m²/s, -29.11 ± 0.14 m²/s and -28.77 ± 0.29 m²/s respectively.

After plotting the graph of $\ln K$ with $1/T$, the growth activation energy and diffusion constant were found from the slope and intercept of the graph and it had a value of 164.78 kJ/mol and $3.86 \times 10^{-14} \text{ m}^2/\text{s}$ respectively.

Furthermore, Zarei *et al.*, (2020) investigated the growth kinetics of aluminide coating developed on HH309 stainless steel by casting and followed by heat treatment process at 950, 975, 1000, 1025 and 1050°C for 0.5, 1, 2, 3, 4 and 5 hours. They calculated the activation energy of the dual-phase structure layer (Fe_2Al_5 and FeAl_2), middle layer (FeAl) and inner layer ($\alpha\text{-Fe(Al)}$) were 203.25 kJ/mol, 249.52 kJ/mol and 246.7 kJ/mol respectively.

In addition, Troysi and Brito (2020) calculated the activation energy of iron aluminide coating formed on mild steel sample at various temperatures (500°C, 550°C, 600°C and 650°C) as shown in Figure 2.11. The activation energy of the coating which contained the Fe_2Al_5 intermetallic layer had a value of 180 kJ/mol was obtained from the growth kinetics of the layer thickness.

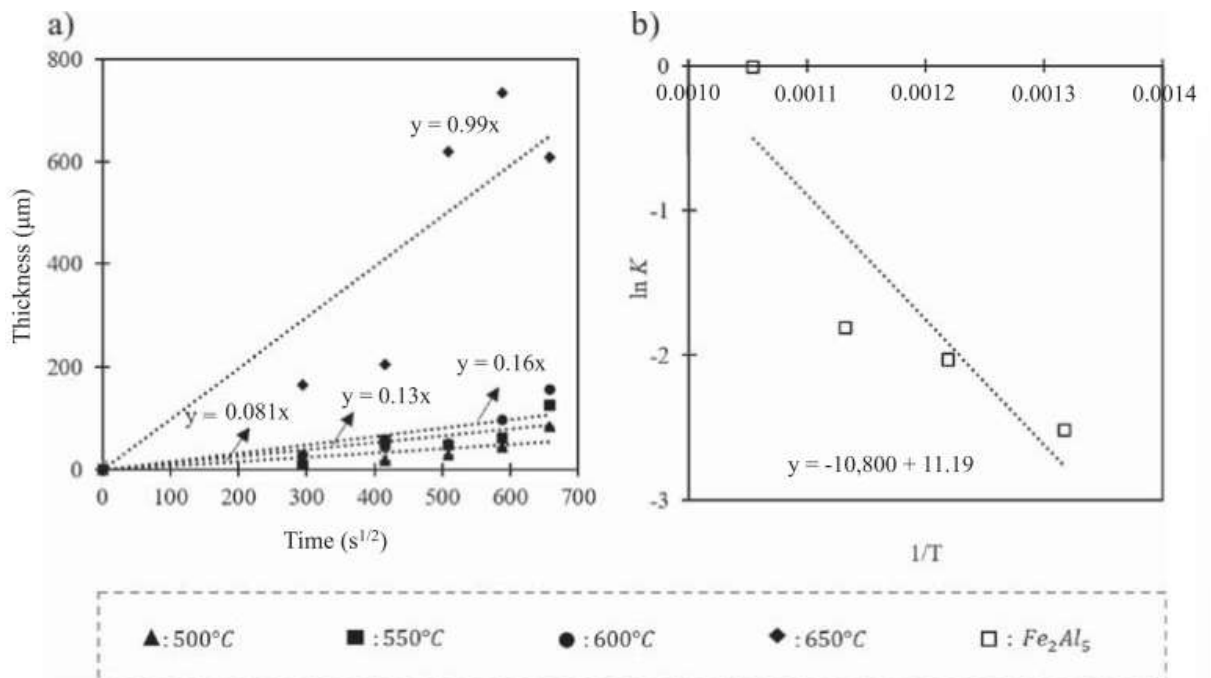


Figure 2.11: Graph of (a) thickness versus time at 500°C, 550°C, 600°C and 650°C and (b) $\ln K$ in the function of $1/T$ (Troysi and Brito, 2020)